PROPERTIES OF MAGNETOPLASMA WAVES IN BISMUTH SINGLE CRYSTALS

M. S. KHAĬKIN, L. A. FAL'KOVSKIĬ, V. S. ÉDEL'MAN, and R. T. MINA

Institute of Physics Problems, Academy of Sciences, U.S.S.R.; Physics Institute, State Atomic Energy Commission, Erevan.

Submitted to JETP editor April 26, 1963

J. Exptl. Theoret. Phys. (U.S.S.R.) 45, 1704-1716 (December, 1963)

Magnetoplasma electromagnetic waves with frequencies 9.5 and 25 Gc propagating in bismuth at helium temperature and in a magnetic field of 0.5—10 kOe are investigated experimentally and theoretically. The qualitative characteristics of the waves are related to the energy spectrum of the current carriers in bismuth.

THE possibility of the propagation of electromagnetic waves inside a metal situated in a constant magnetic field has been the subject of many recent papers [1-11]. In examining this question a distinction must be made between metals having equal and unequal densities of oppositely charged carriers. In the case of inequality, an electromagnetic wave with dispersion $\omega \sim k^2H$ can propagate in the metal, attenuating slightly if $\Omega\tau \gg 1$ ($\Omega = eH/mc$—cyclotron frequency) [1,2]. There are several reports of experimental investigations of waves of this type [2-6].

In the case of equal carrier densities, the situation is different. As shown by Kaner and Skobov [7], the dispersion of electromagnetic waves propagating in such a metal takes the form $\omega \sim kH$, and their attenuation is small when $\omega\tau \gg 1$ (ω—frequency of the wave). These conditions are satisfied by pure bismuth at low temperature. Observation of such waves in bismuth is facilitated by the high value of their velocity $v \approx c\,\Omega/\omega_{pl}$ (this relation will be derived below); the bismuth plasma frequency, on the other hand, is $\omega_{pl} \sim 10^{13}$, which is two orders of magnitude smaller than ω_{pl} for ordinary metals. Indirect confirmation of the existence of such waves is contained in [8-10]. Direct experimental observations of standing electromagnetic waves in plane-parallel bismuth crystals have also been reported [11-13].

Notice must be taken of the essential difference between the considered waves (in the case of equal carrier density) and magnetohydrodynamic Alfven waves, in spite of the outward similarity of their spectra. The former, being collective excitations of electrons, propagate only if $\omega\tau \gg 1$, and are damped as a result of viscosity, whereas the latter call for the opposite condition $\omega\tau \ll 1$, i.e., they exist when hydrodynamics are applicable. We shall therefore call them magnetoplasma waves [13] (many workers [8-11] consider them to be Alfven waves).

The present paper contains a theoretical calculation and an experimental investigation of magnetoplasma waves in bismuth.

THEORY

1. Since we are interested in the connection between the constants that determine wave dispersion and the parameters of the energy spectrum, we present the corresponding calculations.

We use the following coordinates in momentum space: ϵ—energy, p_z—projection of the momentum on the magnetic field ($\mathbf{H} \parallel oz$); $\varphi = eHt/mc$—angle determined by the equations of motion

$$d\mathbf{p}/d\varphi = m\,[\mathbf{vn}], \qquad (1)^*$$

where $\mathbf{n}$—unit vector directed along $\mathbf{H}$

$$m = \frac{1}{2\pi}\frac{\partial S}{\partial \varepsilon} = \frac{1}{2\pi}\oint \frac{dl}{v_\perp},$$

$d\mathbf{l}$—element of the curve $\epsilon = \text{const}$, $p_z = \text{const}$ in p-space. The electric field, as usual, is considered to be small and we confine ourselves in the kinetic equation to the non-equilibrium increment to the distribution function, which is linear in the field and which we write in the form

$$f \sim e^{i(\mathbf{kr}-\omega t)}.$$

The kinetic equation

$$i(\mathbf{kv}-\omega)f + \Omega\frac{df}{d\varphi} = -e\mathbf{v}\mathbf{E}\frac{df_0}{d\varepsilon}$$

$$\left(\Omega = \frac{eH}{mc},\ \mathbf{v}(\varphi, p_z, \varepsilon) = \frac{\partial \varepsilon}{\partial \mathbf{p}}\right)$$

has the following solution that is periodic in φ:

$$f = -\frac{e}{\Omega}\frac{df_0}{d\varepsilon}\int_{-\infty}^{\varphi} \mathbf{E}\mathbf{v}(\varphi')\,d\varphi' \exp\left(i\int_{\varphi'}^{\varphi} d\varphi''\,\omega''/\Omega\right),$$

$$\omega'' = \omega - \mathbf{kv}(\varphi'').$$

*$[\mathbf{vn}] = \mathbf{v} \times \mathbf{n}$.

The conductivity tensor assumes after integration with respect to ϵ, since $-df_0/d\epsilon = \delta(\epsilon - \epsilon_F)$ [1], the form

$$\sigma_{ik} = \frac{2e^2}{(2\pi\hbar)^3}\int \frac{dp_z m}{\Omega}\oint d\varphi\, v_i(\varphi)\int_{-\infty}^{\varphi} d\varphi' v_k(\varphi') \times \exp\left(i\int_{\varphi'}^{\varphi} d\varphi''\,\omega''/\Omega\right). \quad (2)$$

All the quantities are taken here on the Fermi surface.

We represent $\omega - \mathbf{k}\cdot\mathbf{v}$ in the form $\omega - \mathbf{k}\cdot\mathbf{v} = \omega - k_z\bar{v}_z - (\mathbf{k}\cdot\mathbf{v} - k_z\bar{v}_z)$. The bar denotes averaging over φ for specified p_z. The average values $\bar{v}_x = \bar{v}_y = 0$ on the closed trajectories, the only ones present in bismuth. We then obtain

$$\int_{\varphi'}^{\varphi}\omega''\,d\varphi'' = (\omega - k_z\bar{v}_z)(\varphi - \varphi') - \psi(\varphi) + \psi(\varphi'),$$

where

$$\psi(\varphi) = \int_{0}^{\varphi}(\mathbf{kv}'' - k_z\bar{v}_z)\,d\varphi'',$$

and the integration constant can be set here equal to zero, since it cancels out when the difference $\psi(\varphi) - \psi(\varphi')$ is determined.

We now expand the periodic function $v_k(\psi) \equiv v_k(\varphi') \times \exp[i\psi(\varphi')/\Omega]$ in a Fourier series in φ':

$$v_k(\psi) = \sum_n v_k^n(\psi)\, e^{in\varphi'}$$

and we substitute this expansion in σ_{ik}. We get

$$\sigma_{ik} = \frac{e^2}{2\pi^2\hbar^3}\int \frac{dp_z m}{\Omega}\sum_n \frac{v_i^{-n}(-\psi)\,v_k^n(\psi)}{in - i(\omega - k_z\bar{v}_z)/\Omega}. \quad (3)$$

In strong magnetic fields it is necessary to expand σ_{ik} in powers of ω/Ω and kv/Ω. We expand both the denominator of (3) and the numerator in powers of $\psi/\Omega \sim kv/\Omega$. We thus obtain for σ_{zz}

$$\sigma_{zz} = \frac{e^2}{2\pi^2\hbar^3}\int \frac{dp_z m\bar{v}_z^2}{i(k_z\bar{v}_z - \omega)}. \quad (4)$$

We shall henceforth not write out the argument of $v_k(\psi)$ when $\psi = 0$. The function $v_k(\psi)$ with $\psi = 0$ coincides with the true velocity.

In the calculation of $\sigma_{z\alpha}(\alpha = x, y)$ it is necessary to find the next term of the expansion, for the preceeding term (of the type σ_{zz}) vanishes, since $\bar{v}_\alpha = 0$. We have

$$\sigma_{z\alpha} = -\sigma_{\alpha z} = \frac{e^2}{2\pi^2\hbar^3}\int \frac{dp_z m}{\Omega}\left[\frac{\bar{v}_z\cdot\overline{v_\alpha\psi}}{-\omega + k_z\bar{v}_z} + \sum_{n\neq 0}\frac{v_z^{-n}v_\alpha^n}{in}\right]. \quad (5)$$

We now consider the components $\sigma_{\alpha\beta}$. Their terms which are of the order of those written out in (4) and (5) vanish. Indeed, the term similar to the first member in (5) vanishes, again because $v_\alpha = 0$. The term similar to the second component in (5) vanishes when $\alpha = \beta$ because it is odd in n, and σ_{xy} is proportional to the difference of the number of electrons and holes, as can be readily verified by using the definition of φ, and therefore yields zero for sufficiently pure bismuth. Thus, we must calculate the following term of the expansion in $1/\Omega$. Account must be taken of the facts here that $\epsilon(\mathbf{p}) = \epsilon(-\mathbf{p})$, so that the integration with respect to p_z causes the sum

$$k_z\bar{v}_z\sum_{n\neq 0}\frac{1}{in^2}v_\alpha^{-n}v_\beta^n$$

to vanish, as well as the first-order term in ψ/Ω in the expansion

$$\sum_{n\neq 0}\frac{1}{in}v_\alpha^{-n}(-\psi)\,v_\beta^n(\psi).$$

Ultimately we get

$$\sigma_{\alpha\beta} = \sigma_{\beta\alpha} = \frac{e^2}{2\pi^2\hbar^3}\int \frac{dp_z m}{\Omega^2}\left[\frac{\overline{v_\alpha\psi}\cdot\overline{v_\beta\psi}}{i(-\omega + k_z\bar{v}_z)} + \omega\sum_{n\neq 0}\frac{v_\alpha^{-n}v_\beta^n}{in^2}\right]. \quad (6)$$

2. We consider the case of practical importance $\omega \gg k_z v_F$ (v_F—Fermi velocity). Using again the condition $\epsilon(\mathbf{p}) = \epsilon(-\mathbf{p})$ and Eq. (1), we obtain

$$\sigma_{zz} = \frac{e^2}{2\pi^2\hbar^3}\frac{i}{\omega}\int dp_z m\bar{v}_z^2,$$

$$\sigma_{z\alpha} = \frac{e^2}{2\pi^2\hbar^3}\int \frac{dp_z m}{\Omega}\left[\frac{-k_z\bar{v}_z^2\cdot\overline{v_\alpha\psi}}{\omega^2} + \frac{1}{m}\begin{cases}\overline{-v_z(p_y - \bar{p}_y)}, & \alpha = x\\ \overline{v_z(p_x - \bar{p}_x)}, & \alpha = y\end{cases}\right], \quad (7)$$

$$\sigma_{\alpha\beta} = \frac{e^2}{2\pi^2\hbar^3}\int \frac{dp_z m}{\Omega^2} \times\left[\frac{\overline{v_\alpha\psi}\cdot\overline{v_\beta\psi}}{i\omega} + \frac{\omega}{im^2}\begin{cases}\overline{(p_y - \bar{p}_y)^2}, & \alpha = \beta = x\\ \overline{(p_x - \bar{p}_x)^2}, & \alpha = \beta = y\\ \overline{-(p_x - \bar{p}_x)(p_y - \bar{p}_y)}, & \alpha = x,\ \beta = y\end{cases}\right].$$

Maxwell's equations without the displacement currents ($\omega \ll \omega_{pl}$)

$$\mathbf{j} = (ic^2/4\pi\omega)\,[\mathbf{k}\,[\mathbf{kE}]]$$

together with $j_i = \sigma_{ik}E_k$ lead to the dispersion equation

$$\left\|\sigma_{ik} + \frac{ic^2}{4\pi\omega}(k^2\delta_{ik} - k_ik_k)\right\| = 0.$$

Expanding the determinant and omitting terms of the order $(kv/\Omega)^2$, $(\omega/\Omega)^2$, $(kv/\Omega)^2\tan^2\theta$, and $(\omega/\Omega)^2\tan^2\theta$, we obtain

$$\|\sigma_{ik}\| + (ic^2/4\pi\omega)\,[k_z^2(\sigma_{xx}\sigma_{zz} + \sigma_{xz}^2) + k^2(\sigma_{yy}\sigma_{zz} + \sigma_{yz}^2)] - k^2k_z^2\sigma_{zz}(c^2/4\pi\omega)^2 = 0. \quad (8)$$

The coordinate axes are chosen such that k lies in the yz plane.

[1] This is true for sufficiently low temperatures, and is ensured by the stronger condition $\omega\tau \gg 1$. On the other hand, the possible quantum effects are disregarded.

Noting that $\psi \sim k$, we immediately find the form of the solution of (8) (θ—angle between **k** and **H**)

$$\omega = kv(\mathbf{H}, \theta), \tag{9}$$

with

$$v(\mathbf{H}, \theta) \sim c\Omega/\omega_{pl} \tag{10}$$

being a function of the directions of **k** and **h** relative to the crystallographic axes, and to the value of H. We see therefore that a wave excited by an external electromagnetic wave propagates in the metal in a direction normal to the surface ($v(\mathbf{H}, \theta)/c \sim \Omega/\omega_{pl} \ll 1$ in feasible magnetic fields). The component E_z of the electric field is in this wave much smaller than the two others:

$$|E_z/E_{x,y}| \sim \Omega^{-1} \max\{kv_F, \omega\} \ll 1. \tag{11}$$

An explicit form of $v(H, \theta)$ can be obtained for large magnetic fields where $\omega \gg kv_F$. In this case it is necessary to retain in expression (7) for $\sigma_{z\alpha}$ and $\sigma_{\alpha\beta}$ only the second term. In place of (8) we now have

$$Av^4 - H^2v^2(B\cos^2\theta + C)/4\pi + H^4(4\pi)^{-2}F\cos^2\theta = 0. \tag{12}$$

The real constants A, B, C, and F, which depend only on the directions of the magnetic field and the wave vector, and which are determined in all other respects by the energy spectrum of the carriers in the bismuth, are expressed in terms of σ_{ik}:

$$A = (iH^4/\omega c^4)\|\sigma'_{ik}\|, \quad B = H^2c^{-2}(\sigma'_{xx}\sigma_{zz} + \sigma'^2_{xz}),$$
$$C = H^2c^{-2}(\sigma'_{yy}\sigma_{zz} + \sigma'^2_{yz}), \quad F = -i\omega\sigma_{zz}$$

(the primes indicate that only the second terms of $\sigma_{z\alpha}$ and $\sigma_{\alpha\beta}$ of (7) have been retained).

It is seen from (12) that $v(\mathbf{H}, \theta) \backsim H$. One of the solutions of (12) vanishes together with $\cos\theta$. For small values of $\cos^2\theta$ it takes the form

$$v_p^2 = H^2\cos^2\theta F/4\pi C. \tag{13}$$

For the velocity of the second, faster wave we obtain in this case

$$v_s^2 = H^2C/4\pi A. \tag{14}$$

In specific calculations it is necessary to bear in mind that when **H** and **k** lie on symmetry elements, some σ_{ik} vanish. Thus, for example, if the yz plane in which **H** and **k** lie coincides with the symmetry plane, then $\sigma'_{yz} = \sigma'_{yx} = 0$. In this case, for example, $F/C \sim 1/\sigma'_{yy}$.

3. We still have to consider the case $\omega \ll k_z v_F$. Using (4)—(6) it is easy to obtain the asymptotic values of σ_{ik}:

$$\sigma_{zz} = \frac{-ie^2\omega}{2\pi^2\hbar^3k_z^2}\int dp_z m,$$

$$\sigma_{z\alpha} = \frac{e^2}{2\pi^2\hbar^3}\int\frac{dp_z m}{\Omega}\left[\frac{\overline{\psi v_\alpha}}{k_z} + \frac{1}{m}\begin{cases} -\overline{v_z(p_y - \bar{p}_y)}, & \alpha = x \\ \overline{v_z(p_x - \bar{p}_x)}, & \alpha = y \end{cases}\right],$$

$$\sigma_{\alpha\beta} = \frac{e^2}{2\pi^2\hbar^3}\left[\frac{2\pi m\overline{v_\alpha\psi}\cdot\overline{v_\beta\psi}}{\Omega^2|k_z|(\partial\bar{v}_z/\partial p_z)_{\bar{v}_z=0}}\right.$$
$$\left. + \frac{\omega}{i}\int\frac{dp_z}{m\Omega^2}\begin{cases} \overline{(p_y - \bar{p}_y)^2}, & \alpha = \beta = x \\ \overline{(p_x - \bar{p}_x)^2}, & \alpha = \beta = y \\ -\overline{(p_x - \bar{p}_x)(p_y - \bar{p}_y)}, & \alpha = x,\ \beta = y \end{cases}\right].$$

Thus, $\sigma_{\alpha\beta}$ has both imaginary and real parts, leading in general to the absence of undamped waves.

4. We consider a magnetoplasma wave of length λ and frequency ω, propagating with velocity v(H) inside a plane-parallel plate of bismuth of thickness D along a normal to its surface. If the damping of the wave is small and the wave is reflected from the metal surface, then a standing wave is produced in the plate whenever

$$n\lambda/2 = nv(H)/2f = D. \tag{15}$$

Equation (15) is satisfied for selected values of $H = H_n$, consequently the surface impedance of the metal oscillates as the field is varied. If $v(H) = K(\vartheta)H$, where $K(\vartheta)$ is the coefficient that depends only on the angle ϑ and the crystallographic orientation of the plate, then $nH_n = 2Df/K(\vartheta)$ and as a result the oscillations are periodic in the reciprocal field with a period

$$\Delta H^{-1} = H_n^{-1}/n = K(\vartheta)/2Df. \tag{16}$$

EXPERIMENT

The samples were single crystals of bismuth in the form of discs 18 mm in diameter and ~ 0.2—1.7 mm thick, grown from the melt in dismountable polished glass and quartz molds. No subsequent surface treatment was used. The material was bismuth characterized by a resistivity ratio $\rho(300°K)/\rho(4°K) \sim 100$. Some of the specimens were used previously in investigations of cyclotron resonance [12].

During the course of the experiment we continuously measured the parameters of the cavity, one wall of which was the investigated sample. Experiments at 9.5 Gc were carried out with strip resonators, in which a linearly polarized (TEM) wave was excited, so that rectilinear high-frequency currents flowed over the sample surface [14]. The experiments at 24 Gc were carried out with a

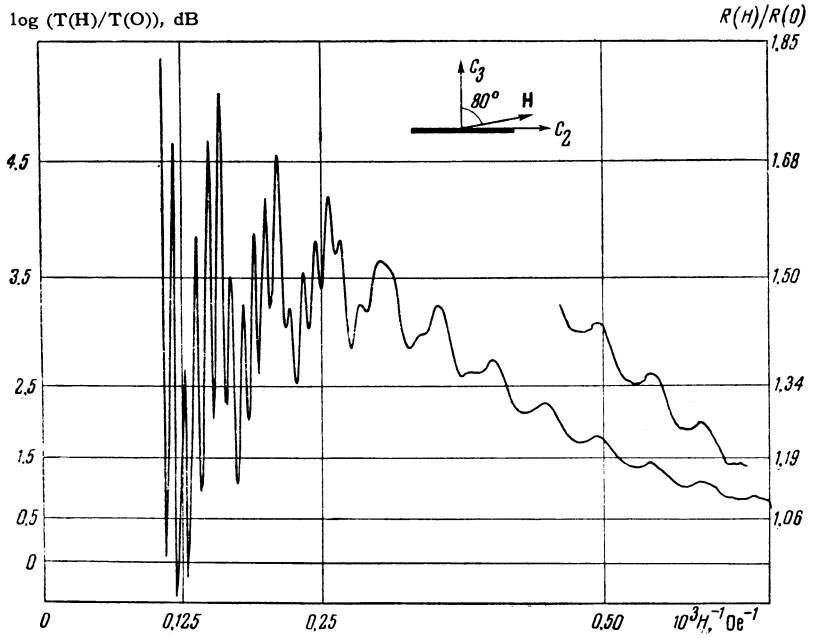

FIG. 1. Plot of the coefficient t = T(H)/T(O) of power transmission through the resonator, demonstrating the simultaneous excitation of magnetoplasma waves of two types: larger period —S waves, smaller period—P waves. The arrangement of the field vector H and the axes C_3 and C_2 in the plane perpendicular to the surface of the sample (Bi-9), which in turn is shown by a solid line, is indicated at the top. On the right is shown part of the curve with greater amplification.

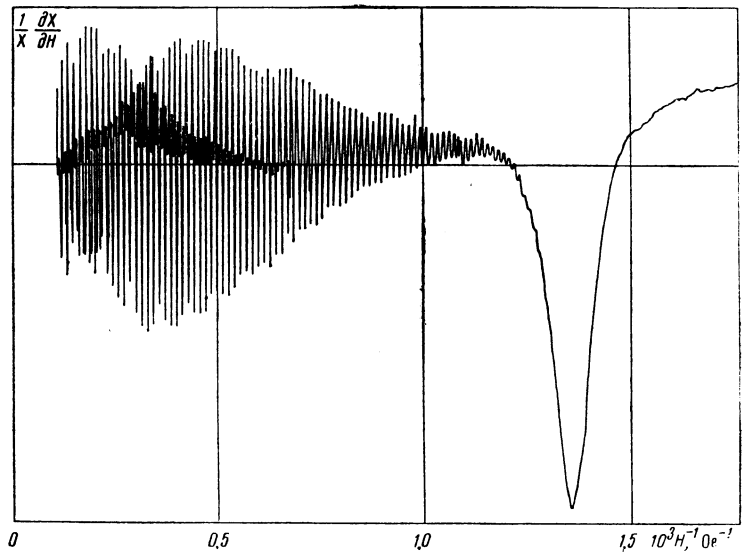

FIG. 2. Plot of periodic S-oscillations for H || C_2 || J. The peak on the right is cyclotron resonance.

cylindrical cavity with the sample as the bottom, operated in the H_{011} or E_{111} mode, so that the currents on the sample surface were respectively circular or curvilinear.

The first observations and the investigations of standing magnetoplasma waves were made by the frequency modulation method [14]; however, when the surface-impedance oscillations caused by them reached a large amplitude, the use of a sensitive measurement procedure became not only unnecessary, but also impossible. In such cases the measurements were made by recording the coefficient of power transfer through the resonator containing the sample [15]. The sample temperature was usually 1.8°K. The magnetic field was rotated in the experiments at 9.5 and 25 Gc in the plane of the specimen, and could be inclined to the latter by ± 1.5—2°. In experiments at 9.5 Gc, using the Bi-9 sample, the magnetic field was also rotated in a plane perpendicular to the sample surface. The high-frequency current was in the same plane.

Typical records of oscillations obtained during the course of the experiments for the logarithmic derivative of the surface impedance of bismuth and its surface resistance, as functions of the reciprocal of the magnetic field, are presented in [13] and also in Figs. 1—4. In all cases when the magnetic field was parallel to the sample surface, oscillations of one period, called S-oscillations, were observed. If the field was inclined to the surface of the sample, then oscillations with a smaller period were observed, having different properties

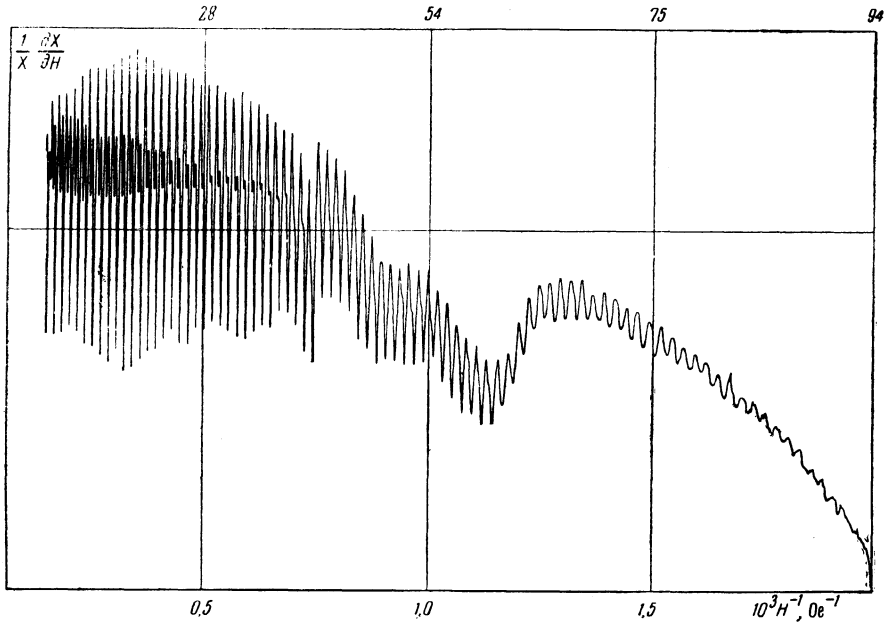

FIG. 3. Plot of aperiodic S-oscillations for **H** || C_3 || **J**. The numbers on the top denote the serial numbers n of the oscillations, counting from $H^{-1} = 0$.

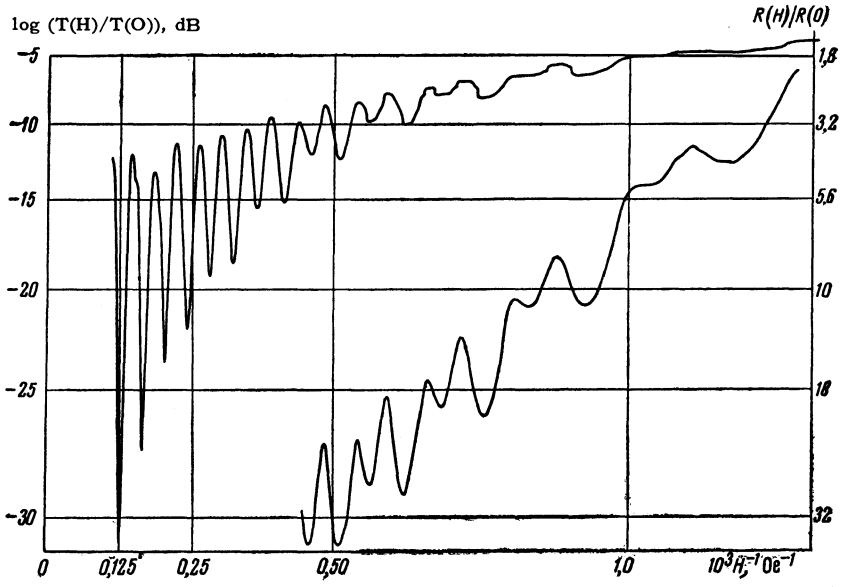

FIG. 4. Plot of aperiodic P-oscillations for H || N, in the Bi-9 sample (⊄ N, $C_3 \approx 4°$). Lower curve—same plot with greater amplification.

and called P-oscillations. Figure 1 shows a case of simultaneous observation of oscillations of both types. The corresponding magnetoplasma waves are called S waves or P waves.

PROPERTIES OF MAGNETOPLASMA S WAVES

A characteristic feature of S-oscillations, observed in all experiments for any crystallographic sample orientation, is the dependence of their amplitude on the angle between the field **H** and the high frequency current **J**. When **H** || **J**, the amplitude of the oscillations is minimal and increases rapidly with increasing angle between H and J. Additional minima of smaller amplitude, which are always seen in the intervals between the principal minima (Fig. 2 of [13]), disappear almost completely when **H** || **J** (Figs. 2 and 3). The amplitude of the oscillations increases approximately as $T^{-(1-1.5)}$.

The S-oscillations of surface impedance of samples having an orientation **N** || C_3 are periodic within the limits of measurement accuracy, as is seen, for example, from Fig. 2. The measured anisotropy ΔH^{-1} of the field H as it is rotated in the plane of the surface of the single crystal is shown in Fig. 5, where the interpolation curve corresponds to the equation

$$1/\Delta H^{-1} = (27.3 + \cos 6\alpha)\, 3.14 \quad \text{kOe}.$$

For samples whose surface plane contains the

Table I

Field direction	Sample	∢N, C_3	D, mm	f, Gc	ΔH^{-1}, 10^{-4} Oe^{-1}	$vH^{-1} = 2Df\Delta H^{-1}$, 10^4 cm·sec^{-1}·Oe^{-1}
H ∥ C_2	Bi-1	87°	1.74±0.01	9.51±0.01	1.41±0.02	4.65±0.1
	Bi-4	90°	1.74±0.01	9.47±0.01	1.39±0.02	4.60±0.1
	Bi-4	90°	1.74±0.01	25.0 ±0.01	0.56±0.02	4.8 ±0.2
	Bi-2	1°	1.74±0.01	9.55±0.01	1.13±0.02	3.75±0.1
	Bi-3	2°	1.74±0.01	9.50±0.01	1.13±0.02	3.75±0.1
	Bi-6	0°	1.73±0.01	9.53±0.01	1.13±0.02	3.70±0.1
	Bi-7	38°	0.98±0.01	9.51±0.01	2.13±0.03	4.0 ±0.1
	Bi-9	3°	0.47±0.01	9.53±0.01	4.06±0.06	3.65±0.15
	Bi-9	3°	0.47±0.01	24.85±0.01	1.38±0.02	3.20±0.15
	Bi-16	0°	0.19±0.005	9.43±0.01	10.7±0.1	3.83±0.15
H ∥ C_1	Bi-11	90°	0.98±0.01	9.52±0.01	6.40±0.1	11.95±0.2
	Bi-11	90°	0.98±0.01	21.10±0.01	2.90±0.05	12,0 ±0.2
	Bi-11	90°	0.98±0.01	27.07±0.01	2.22±0.05	11.8 ±0.2

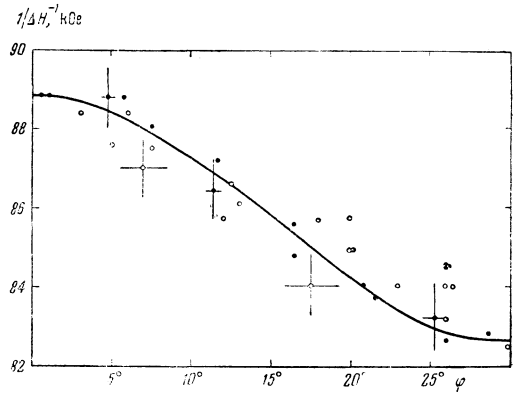

FIG. 5. Anisotropy of S-oscillations in the bismuth crystal basal plane. Circles—measurements with Bi-2 sample with the field rotation limited to 120°; black dots—Bi-3 with 65° limit. All data are reduced to the angle interval $\alpha \leq 30°$, measured from the C_2 axis. The bars at some points denote measurement errors.

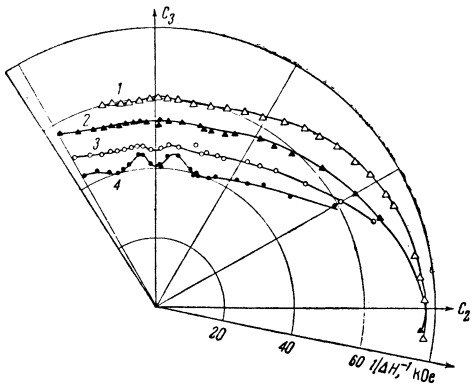

FIG. 6. Anisotropy of S-oscillations in the plane containing the axes C_2 and C_3 of Bi-4 sample. The period ΔH^{-1} is calculated as the average over the interval H^{-1}; curve 1—H^{-1} in the interval $(0 - 0.5) \times 10^{-3}$ Oe^{-1}; 2—$(0.5 - 1) \times 10^{-3}$ Oe^{-1}; 3—$(1 - 1.5) \times 10^{-3}$ Oe^{-1}; 4—$(1.5 - 2) \times 10^{-3}$ Oe^{-1}.

axes C_2 and C_3, the period of the S-oscillations turns out to be dependent on the field, but to a different extent for different field directions. The case **H** ∥ C_3 is illustrated in Fig. 3. The anisotropy of the period can be judged from Fig. 6, from which we can see, in particular, that the aperiodicity of the S-oscillations is most noticeable at field directions **H** close to the C_3 axis.

In order to clarify the nature of the observed oscillations, experiments were carried out with samples of different thickness and at different frequencies. It has been established as a result that $\Delta H^{-1} \backsim (Df)^{-1}$ or, as can be seen from Table I, $Df\Delta H^{-1}$ = const, within measurement accuracy, for thicknesses that differ by a factor of 9, and for frequencies that differ by a factor 2.5.[2)] This confirms the correctness of relationship (16), derived on the basis of the notion of standing waves in the sample. It must be noted that the fact that samples differing in normal orientation have S-oscillation periods that differ by ~20 per cent when **H** ∥ C_2 (see Table I) also confirms that the observed effect is due to formation of standing magnetoplasma waves.

If the magnetic field is inclined to the surface of the sample, then the amplitude of the S-oscillations decreases, but to a different degree depending on the crystallographic orientation of the plane in which the field **H** is rotated. The change in periods which occurs in this case is indicated in Fig. 7.

PROPERTIES OF MAGNETOPLASMA P WAVES

Magnetoplasma P-oscillations were investigated with the Bi-9 sample. Figure 2 of [13] shows a plot of the power transfer coefficient $t = T(H)/T(0)$ at the field direction causing the strongest P-oscillations. The magnetic field lies in this case in the diagonal crystallographic plane σd.

An analogous plot, but with the field vector lying in the plane containing the axis C_2 and C_3 is shown in Fig. 1. The losses in the resonator are deter-

[2)] A discrepancy exceeding the experimental error occurs in one case: when H || C_2 and N || C_3, in the Bi-9 sample; the reason for it is not yet clear.

mined almost completely by the losses in the bismuth sample, so that the experiment yields directly the relative increase in the surface resistance of the bismuth $R(H)/R(0)$ at resonant values of the field.

When the direction of the vector **H** lies in some region close to the direction of the C_3 axis, then the P-oscillations are strongly aperiodic, as is seen, for example, in Fig. 4. However, in other cases the period of the P-oscillations depends little on the field, as is illustrated, in particular, by Figs. 1 and 2 of [13].

The most distinguishing feature of the P-oscillations is the dependence of their period, calculated from the formula $\Delta H^{-1} = H_n^{-1}/n$, on the angle ϑ between the direction of the magnetic field **H** and the normal N to the sample surface. In Fig. 7 this dependence is shown for two crystallographic planes. With the exception of a small interval of directions close to the C_3 axis ($\vartheta \lesssim 30°$), the experimental points on the diagrams of Fig. 7 fall on straight lines. (When **H** has nearly the same direction as C_3, the S-oscillations also display maximum anisotropy and aperiodicity—see above).

Using this fact, we can separate the dependence of the period of the P-oscillations $\Delta_P H^{-1}$ on the angle between **H** and **N** into two parts: 1) anisotropy determined by the orientation of the vector H relative to the crystal axes, and 2) dependence on the angle between the vectors of the field H and the velocity v. Inasmuch as $\mathbf{v} \parallel \mathbf{N}$, we obtain for the experimental lines of Fig. 5 $\Delta_P H^{-1}(\vartheta) = \Delta_P^0 H^{-1} \cos\vartheta$.

In the case of Fig. 7b, in the interval $\vartheta \leq 20°$, we see simultaneously two types of oscillations; the character of their anisotropy is the same in this angle interval. (We note the similarity between the anisotropy of the periods of the S- and P-oscillations, shown in Fig. 7b and Fig. 6.) From considerations which will be advanced during the discussion of the results, and also by using the extrapolation of which Fig. 7 admits, we shall assume the oscillations with the large period in Fig. 7 to be S-oscillations, while the others, which show a dependence of the type $\Delta H^{-1}(\vartheta) = \Delta^0 H^{-1} \cos\vartheta$, will be regarded as P-oscillations.

The difference in the periods ΔH^{-1} for P-oscillations when $\mathbf{H} \parallel \mathbf{N}$ (Fig. 7a and 7b) can be attributed to error in the orientation of the normal to the sample relative to the plane in which the magnetic field is rotated. It is seen from Fig. 7a that an error of 1.5—2° can cause such a difference in the periods.

DISCUSSION OF RESULTS

From the experimental data shown in the figures and in Table I, we obtain from (15) and (16) the numerical characteristics of S-waves:

$$v_S = (2 - 50)\cdot 10^7 \text{ cm/sec},$$
$$\lambda_S = 0.02 - 0.5 \text{ mm}; \quad n = 2 - 100. \qquad (17)$$

We note that the maximum value of v_S is determined by the magnitude of the field of the electromagnet used in the experiments ($H < 10$ kOe). The velocity v_P of the P waves is always smaller than v_S. Thus, the greatest velocity of magnetoplasma waves in the above experiments is two orders of magnitude smaller than the velocity of light, in agreement with the estimate resulting from Eq. (10): $v(10 \text{ kOe}) \approx c/30$. This causes the magnetoplasma waves to propagate normally to the surface of the metal (this was used in the derivation of (15)) independently of the angle of incidence of the exciting electromagnetic wave.

A consequence of the theory is the smallness of the component of the electric field E_H in the magnetoplasma wave compared with the other components of **E**. This means that the worst excitation conditions occur when $\mathbf{H} \parallel \mathbf{J}$, which is fully confirmed by the experiments.

To confirm the correctness of the linear dispersion law (9), which follows from the theory, it is sufficient to verify that the velocity v does not depend on f. In the case of periodic oscillations this reduces to a verification of the relationship

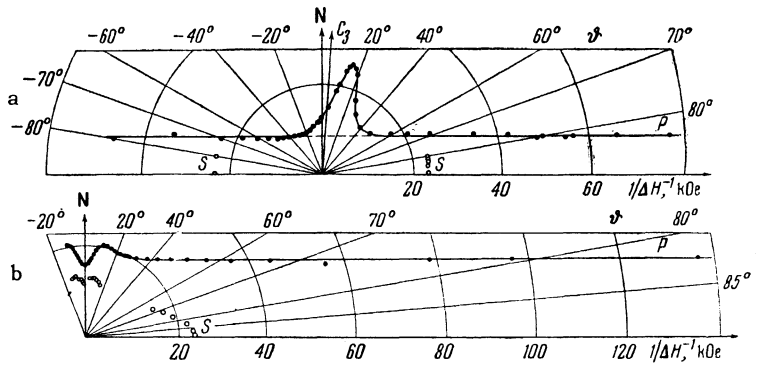

FIG. 7. Dependence of the periods of the S- and P-oscillations on the angle θ for the Bi-9 sample: a—plane σ_d; b—plane containing the axes C_2 and C_3.

$\Delta H^{-1} f$ = const, as can be seen from (16). The results of the experiments given in Table I confirmed the correctness of this relationship.

We have compared above the experimental results with theoretical deductions that are valid if $k_H v_F \ll \omega$. At large values of the magnetic fields, a more stringent condition $kv_F \ll \omega$ is satisfied, but taking into account the estimates of (17) given for λ, even this condition is satisfied for the greater part of the field interval in which oscillations are observed. As follows from (12), we have here $v \backsim H$ and the oscillations are periodic. It follows from the experiment that the S- and P-oscillations are as a rule periodic (Figs. 1 and 2 and [13]). Aperiodicity appears only when the direction of H is close to that of the C_3 axis. Incidentally, as is seen from Figs. 3 and 4, the periodicity improves towards larger fields, which agrees with the deductions of the theory.

It follows from (12) that two waves can propagate in bismuth when $\vartheta \neq 90°$, and only one when $\vartheta = 90°$. This is fully confirmed by experiment (Figs. 1—3), and has served as a basis for separating the experimentally observed oscillations into two types, called S- and P-oscillations. These considerations were taken into account above in the description of the results of the experiments for $\mathbf{H} \parallel C_3$ (Fig. 7).

The theoretical dependence of the velocities of the S and P waves on the angle ϑ for small values of $\cos\vartheta$ is represented by (13) and (14). The correctness of these relationships follows from the experimental results shown in Fig. 7. The interval of values in which (13) and (14) are confirmed is determined by the anisotropy of the wave velocity in the plane of rotation of the magnetic field H.

Let us calculate from (13) and (14) the values of the velocities of the S and P waves for some orientations of k and H. When $\mathbf{k} \parallel C_3$ and $\mathbf{H} \parallel C_1$ or $\mathbf{H} \parallel C_2$, we obtain for the ratio C/A contained in the expression for v_S, respectively,

$$\frac{C}{A} = \frac{\omega c^2}{iH^2} \frac{\sigma'_{11}(1)}{\sigma'_{22}(1)\,\sigma'_{11}(1) + \sigma'^2_{21}(1)}$$

$$(\mathbf{H} \parallel C_1,\ \sigma'^2_{13}(1) = \sigma'_{23}(1) = 0), \tag{18}$$

$$\frac{C}{A} = \frac{\omega c^2}{iH^2} \frac{\sigma'_{33}(2)}{\sigma'_{11}(2)\,\sigma'_{33}(2) - \sigma'^2_{13}(2)}$$

$$(\mathbf{H} \parallel C_2,\ \sigma'_{12}(2) = \sigma'_{23}(2) = 0). \tag{19}$$

The coordinate axes are connected with the crystallographic directions: the subscripts 3, 2, and 1 denote the directions C_3 and C_2, and the direction C_1 which is perpendicular to them.

Estimating the contributions of the electrons and the holes in σ'_{ik} on the basis of the experimental data relating to the effective masses m [12] and the cross sections S_{extr} of the Fermi surface [16], we find that the major role is played in this case by the holes, with $\sigma'^2_{13}(2) \ll \sigma'_{11}(2)\,\sigma'_{33}(2)$ and $\sigma'^2_{21}(1) \ll \sigma'_{22}(1)\,\sigma'_{11}(1)$. The quantities $\sigma'_{11}(2)$ and $\sigma'_{22}(1)$ remaining in (18) and (19) take the form

$$\sigma'_{11}(2) = \frac{4\pi c^2\omega}{i(2\pi\hbar)^3 H^2} \int dp_2 \cdot \overline{p_3^2 m}(2),$$

$$\sigma'_{22}(1) = \frac{4\pi c^2\omega}{i(2\pi\hbar)^3 H^2} \int dp_1 \cdot \overline{p_3^2 m}(1).$$

Taking into account the axial symmetry of the hole Fermi surface [12,16] we get $\sigma'_{11}(1) = \sigma'_{22}(2)$. This leads to an equality of the corresponding velocities, as does occur experimentally (Table II, Fig. 5) with accuracy ~ 10 per cent, corresponding to the computational accuracy.

In the case when $\mathbf{H} \parallel C_1$ and $\mathbf{k} \parallel C_3$ we obtain for $\sigma'_{33}(1)$, which determines v_P,

$$\sigma'_{33}(1) = \frac{4\pi c^2\omega}{i(2\pi\hbar)^3 H^2} \int dp_1 \cdot \overline{p_2^2 m}(1),$$

where the main contribution is again made by integration over the hole Fermi surface.

An estimate shows that [16]

$$\sigma'_{33}(1)/\sigma'_{22}(1) = [S_{extr}(3)/S_{extr}(2)]^2 \approx 9;$$

Table II

	S waves		P waves	
	vH^{-1}, 10^4 cm·sec^{-1}·Oe^{-1}		$vH^{-1}/\cos\theta$, 10^4 cm·sec^{-1}·Oe^{-1}	
	Experiment	Theory*	Experiment	Theory*
$\mathbf{H} \parallel C_2$, $\mathbf{k} \parallel C_3$	3.7±0.1	2.2	5.2±0.1	2.7
$\mathbf{H} \parallel C_2$, $\mathbf{k} \parallel C_1$	4.6±0.1	2.7	—	—
$\mathbf{H} \parallel C_1$, $\mathbf{k} \parallel C_3$	4.0±0.1	2.2	11.1±0.2	6.7
$\mathbf{H} \parallel C_1$, $\mathbf{k} \parallel C_2$	12,0±0.2	6.7	—	—

*Calculated on the ellipsoidal model.

in which case the corresponding velocities $v_P\cos\vartheta$ and v_S should differ by $(\sigma'_{33}(1)/\sigma'_{22}(1)^{1/2} = 3$ times. Experiment, on the other hand, gives a velocity ratio of 2.8 (Table II).

For the velocity v_S when $\mathbf{H} \parallel C_1$ and $\mathbf{k} \parallel C_2$ we obtain a value coinciding with $v_P/\cos\vartheta$ for $\mathbf{H} \parallel C_1$ and $\mathbf{k} \parallel C_3$.

We now consider the cases $\mathbf{H} \parallel C_2$, $\mathbf{k} \parallel C_3$ and $\mathbf{k} \parallel C_1$. An estimate shows that the corresponding velocities $v_P/\cos\vartheta$ and v_S are determined by the electrons and are equal, in agreement with experiment (Table II).

Table II gives the results of calculations of the velocities v_S and v_P under the assumption that the spectrum of the holes and of the electrons is quadratic (the reciprocal of the electron mass tensor was taken from the article by Weiner [17]). The considerable discrepancy between the results obtained and the experimental data can be attributed to the essential difference between the two energy spectra of bismuth and the model employed.

It must be noted that the effect under consideration is integral and, in an analogy with specific heat, calculation of v_S and v_P using the ellipsoidal model gives results that differ noticeably from the measured quantities. At the same time, a calculation of the ratio of the velocities, which is not based on the model, leads to results that almost coincide with the experimental values.

The authors are grateful to P. L. Kapitza for interest and collaboration, to A. A. Abrikosov for a discussion, and to G. S. Chernyshev and V. A. Yudin for technical help.

[1] O. V. Konstantinov and V. I. Perel', JETP 38, 161 (1960), Soviet Phys. JETP 11, 117 (1960).

[2] Bowers, Legendy, and Rose. Phys. Rev. Lett. 7, 339 (1961).

[3] Rose, Taylor, and Bowers. Phys. Rev. 127, 1122 (1962).

[4] Cotti, Wyder, and Quattropani. Phys. Lett. 1, 50 (1962).

[5] Taylor, Merrill, and Bowers. Bull. Amer. Phys. Soc. II. 8, 65 (1963).

[6] R. G. Chambers and B. K. Jones. Proc. Roy. Soc. A270, 417 (1962).

[7] É. A. Kaner and V. G. Skobov. JETP 45, 610 (1963), Soviet Phys. JETP 18, 419 (1964).

[8] S. J. Buchsbaum and J. K. Galt, Phys. Fluids, 4, 1514 (1961). Galt, Yager, Merritt, and Cetlin. Phys. Rev. 114, 1396 (1959).

[9] J. Kirsch and P. B. Miller. Phys. Rev. Lett. 9, 421 (1962).

[10] P. B. Miller and R. R. Hering. Phys. Rev. 128, 126 (1962).

[11] J. Kirsch. Bull. Amer. Phys. Soc. II, 8, 205 (1963).

[12] Khaĭkin, Édel'man and Mina. JETP 43, 2063 (1962); Soviet Phys. JETP 16, 1459 (1963); Paper at the Ninth All-Union Conference on Low-Temperature Physics, Leningrad, July 1962.

[13] Khaĭkin, Édel'man, and Mina. JETP 44, 2190 (1963), Soviet Phys. JETP 17, 1470 (1963).

[14] M. S. Khaĭkin. PTE No. 3, 95 (1961).

[15] R. T. Mina. JETP 40, 1293 (1961), Soviet Phys. JETP 13, 911 (1961).

[16] N. B. Brandt. JETP 38, 1355 (1960), Soviet Phys. JETP 11, 975 (1960).

[17] D. Weiner. Phys. Rev. 125, 1226 (1962).

Translated by J. G. Adashko
272